Optimal discretization of grounding systems applying Maxwell's subareas method

Optimal discretization of grounding systems applying Maxwell's subareas method

Pasquale Montegiglio, Giuseppe Cafaro, Francesco Torelli
Department of Electrical and Information Engineering
Polytechnic University of Bari
Bari, Italia
pasquale.montegiglio@poliba.it

Pietro Colella, Enrico Pons
Energy Department
Polytechnic University of Torino
Torino, Italia
pietro.colella@polito.it

***Abstract*— This paper presents a method for evaluating the optimal number n of equivalent sources needed for simulating grounding systems by the Maxwell's subareas method. It is well known that the number of elements in which electrodes are subdivided plays a role on the accuracy and reliability of results (as well as on computational time). Previous studies, accomplished through iterative calculations (performed with different segmentations), led mostly to some recommended practices for the identification of lower and upper bounds for n. The procedure proposed in this paper allows for predicting the optimal n in a single process. The method starts from the identification of a set of appropriate scalar functions, which heuristically express a relation between the number of subareas and the accuracy of the results (earth resistance and earth surface voltages) computed applying the Maxwell's subareas method. Then, a multi-objective optimization process evaluates the number n^* that maximizes that accuracy.**

Keywords— Maxwell's subareas method, grounding system modeling, grounding, ground resistance, Finite Element Method (FEM), discretization.

I. INTRODUCTION

The study of most industrial grounding systems can be carried out employing the Maxwell's Subareas Method (MaSM) [1]-[5]. According to MaSM, the quasi-static model of a generic grounding electrode can be obtained starting from its subdivision into a number n of cylindrical segments (named *subareas*) characterized by the following properties:

1. having a length adequately greater than their diameter;
2. being at the same potential under fault conditions.

The occurrence of condition 1 allows for assuming the current field generated by each segment as produced by a uniform linear current source laying on its longitudinal axis. Condition 2 states that the voltage drop along conductors making up the considered ground electrode is negligible.

Fig. 1 shows an example of discretization (in n subareas) of a simple cylindrical electrode embedded in a conductive homogeneous medium.

Every single segment interacts with the others by means of voltage coefficients R_{ij} [5]. Each R_{ij} represents the voltage produced by the inducing subarea j in the C_i barycentre of the induced subarea i, when j is leaking a unitary current.

In order to have a good representation of the nonuniform current distribution along the overall electrode [6]-[9], n must be properly chosen. Since each subarea is modelled as a uniform linear current source, from a theoretical point of view, a larger n should result in a more adequate representation of the leakage current distribution.

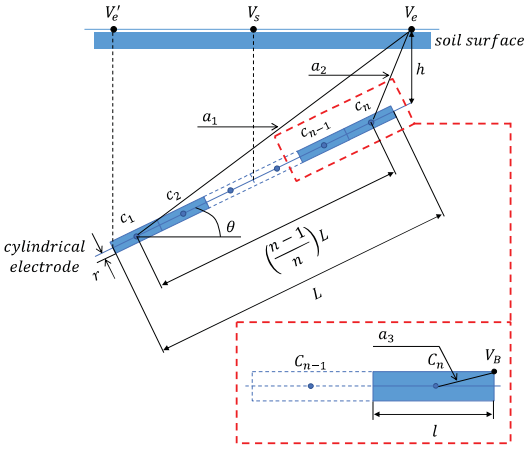

Fig. 1. Cylindrical electrode subdivided in n equivalent sources (i.e. subareas)

However, if n is increased over a certain value, the length of each segment becomes comparable with its radius, making condition 1 no longer satisfied. Therefore, there are two opposite requirements placing a limit on the accuracy of the final solution:

- the requirement for a good approximation of the leakage current distribution along the electrode, which is a lower bound on n;
- the requirement stated by condition 1, which is an upper bound on n.

Previous studies focused on the role of n and its appropriate choice. Paper [6] discussed issues encountered in the simulation of grounding systems using a semi-analytical method quite similar to the MaSM (the Average Potential Method), showing the effect that segmentation has on the model predictions. Authors conclude that models based on the afore mentioned method should be iteratively simulated, increasing the number of subareas per computer run in order to determine the adequacy of the adopted segmentation.

In [7], results of computational error analyses related to the segmentation of simple ground conductors are reported. The analysis procedure is accomplished by iterative calculations. When an increased segmentation produces no significant change in the computed quantities (i.e. earth resistance of the electrode and soil surface potential), the "right" number of subareas $\bar{N}$ can be assumed. Authors propose recommended

practices to determine, case by case, a range of feasible values for n.

In [8] it is shown that, using just one segment (i.e. $n = 1$) to represent a long rod (20 m length) buried in a homogeneous medium, the calculation of the voltage on the surface of the conductor (which should be constant) is not accurate (10 to 20% error) and the largest errors are located at the rod ends. In order to improve accuracy and substantially restore the constant voltage along the rod, a sphere is added at both ends of the rod. It is also proved that the relative error on the potential decreases as the distance from the conductor boundary increases. In other words, the error decreases from its maximum value, which is located at the boundary of the conductor, to zero at infinity.

A fuzzy approach aiming at the *a priori* estimation of errors in the evaluation of the voltage coefficients R_{ij} for a chosen rate of subdivision, is proposed in [9]. The method starts from the prior knowledge of $\overline{N}$. Then a calculation of the error on coefficients R_{ij}, for a chosen $n < \overline{N}$, is performed by fuzzy logic. According to the value of this error, it is possible to decide whether the number n can be accepted or if it should be increased. As previously mentioned, this procedure, specially intended to perform faster computations (and to save memory) reducing the number of subdivisions, requires the a priori knowledge of $\overline{N}$, which is determined through iterative calculations.

In this paper, a procedure for evaluating the optimal number of subareas in *one shot* (i.e. without need for iterative simulations of the grounding electrode model) is proposed. Based on conclusions and results presented in literature, a set of appropriate scalar functions have been identified; each scalar function expresses, in a heuristic way, a relation between the number of subareas and the accuracy of the model predictions. Proposed functions are then processed by a Multi-objective Optimization (MO) procedure, in order to evaluate the number n^* that maximizes the accuracy.

In the following Sections the objective functions and the optimization algorithm are presented. The method is then applied to a simple case study in order to test its performances.

II. Objective Functions

As stated in the previous Section, within the limits imposed by condition 1, a model based on the MaSM will surely be more accurate if the electrode under study is subdivided into smaller and smaller segments [6]. This can have an intuitive understanding: the evaluation of the generic voltage coefficient R_{ij}, between the inducing subarea i and the induced subarea j, is based on the assumption that the latter can be approximated to its barycentre C_j, instead of being considered l long (see Fig. 1). When n decreases, the length of each subarea turns to be greater and, as a consequence, the abovementioned approximation will involve larger errors on R_{ij} [9].

Therefore, it is possible to state that the accuracy of the results is proportional to the reciprocal of subareas length:

$$Acc_1 \propto \frac{1}{l} = \frac{n}{L} \,, \tag{1}$$

where L is the total length of the electrode.

Moreover, it comes from intuition that approximating a generic induced subarea j to its barycentre produces - for a chosen n - an error on R_{ij} that increases as the distance $\overline{C_i\, C_j}$ decreases [9]. This means that the accuracy on the evaluation of the mutual interference between the subareas located at the extremities of the considered conductor (identified by C_1 and C_n in Fig. 1), is proportional to their barycentric distance:

$$Acc_2 \propto (n-1)l = \frac{(n-1)L}{n} \,. \tag{2}$$

As demonstrated in [8], the relative error on the electric potential computed in a generic point of the soil decreases as the distance of that point from the boundary surface of the conductor increases. This implies that the accuracy on the evaluation of the electric potential induced on the soil surface is proportional to the distance of the electrode from the soil surface. With reference to Fig. 1, in order to fully characterize the conductor position with respect to the ground surface, two distances - namely a_1 and a_2 - have been considered.

Therefore, it can be stated that accuracy increases proportionally with increasing a_1 and a_2. By considering the *law of cosines*, it is possible to write the following relations:

$$Acc_3 \propto a_1 = \sqrt{k_1^2 L^2 + h^2 - 2hLk_1 cos\left(\frac{\pi}{2} + \theta\right)} \,, \tag{3}$$

$$Acc_4 \propto a_2 = \sqrt{k_2^2 L^2 + h^2 - 2hLk_2 cos\left(\frac{\pi}{2} + \theta\right)} \,, \tag{4}$$

where h and θ, respectively, are the burial depth and burial angle of the considered electrode (see Fig. 1). Moreover, $k_1 = (2n-1)\,/\,2n$, and $k_2 = 1\,/\,2n$.

Finally, it can be stated that the accuracy on the evaluation of potential V_B on the boundary of the conductor (see detail in Fig. 1) increases as the conductor radius r decreases. This has an intuitive understanding too: the modeling assumption that each segment of the grounding electrode can be considered as a linear current source will necessarily involve larger errors for larger conductor radii. Therefore, it is possible to write what follows:

$$Acc_5 \propto \frac{1}{a_3} = \frac{1}{\sqrt{k_2^2 L^2 + r^2}} \,. \tag{5}$$

In this Section, a set of five scalar nonlinear equations has been identified, which states - for a given conductor - the dependence of the model accuracy on the number of subareas n. The goal is to find the optimal n^* that simultaneously maximizes all the expressions in the set. This can be achieved through a MO process aimed at finding the minimum of the reciprocals of equations (1)-(5).

III. Optimization Algorithm

A. Problem Formulation

From a mathematical perspective, a MO problem requires the simultaneous minimization of several scalar functions $f_i(\boldsymbol{z})$. By denoting with $\boldsymbol{z} = \left[z_1, z_2, \ldots, z_{m_4}\right]^T$ the vector of

unknown variables, the general formulation of the problem is the following:

$$\begin{cases} \min\limits_{\boldsymbol{z}} f_i(\boldsymbol{z}) & i = 1,2,\dots,m_1 \\ s.t.\ g_j(\boldsymbol{z}) = 0 & j = 1,2,\dots,m_2 \\ u_k(\boldsymbol{z}) \le 0 & k = 1,2,\dots,m_3 \\ z_{p,min} \le z_p \le z_{p,Max} & p = 1,2\dots,m_4 \end{cases} \quad (6)$$

where m_1 is the number of scalar objective functions and m_2 is the number of equality constraints. The inequality constraints include the minimum and maximum for each element of $\boldsymbol{z}$ and constraints $u_k(\boldsymbol{z})$.

It can be observed that the minimization of the objective function vector $\boldsymbol{f}(\boldsymbol{z}) = \left[f_1, f_2, \dots, f_{m_1}\right]^T$ is equivalent to find the zeros of the following error function vector:

$$\boldsymbol{f}(\boldsymbol{z}) - \boldsymbol{q} = \boldsymbol{0} \quad (7)$$

where $\boldsymbol{q}$ is an additional unknown vector representing the minimum of the function $\boldsymbol{f}(\boldsymbol{z})$.

According to the *Interior Point Theory*, inequality constraints can be converted into equality constraints by introducing nonnegative slack variables [10]-[12]. Consequently, they can be recast as follows:

$$\begin{cases} \boldsymbol{u}(\boldsymbol{z}) + \boldsymbol{s} - \boldsymbol{h_{Max}} = \boldsymbol{0} \\ \boldsymbol{u}(\boldsymbol{z}) - \boldsymbol{t} - \boldsymbol{h_{min}} = \boldsymbol{0} \end{cases} \quad (8)$$

where $\boldsymbol{s}$ and $\boldsymbol{t}$ are two additional unknown vectors representing nonnegative slack variables.

Summarizing, it is possible to identify the following vector of objective functions:

$$\begin{cases} \boldsymbol{E}_1 = \boldsymbol{f}(\boldsymbol{z}) - \boldsymbol{q} \\ \boldsymbol{E}_2 = \boldsymbol{g}(\boldsymbol{z}) \\ \boldsymbol{E}_3 = \boldsymbol{u}(\boldsymbol{z}) + \boldsymbol{s} - \boldsymbol{h_{Max}} \\ \boldsymbol{E}_4 = \boldsymbol{u}(\boldsymbol{z}) - \boldsymbol{t} - \boldsymbol{h_{min}} \end{cases} \quad (9)$$

The target is finding the values of the dependent $\boldsymbol{z}$ and slack $\boldsymbol{q}$, $\boldsymbol{s}$, $\boldsymbol{t}$ variables that make equal to zero, at the same time, each of the (9). This may be expressed, in a compact form, as follows:

$$\boldsymbol{E}(\boldsymbol{v}) = \boldsymbol{0} \quad (10)$$

where $\boldsymbol{E} = [\boldsymbol{E}_1, \boldsymbol{E}_2, \boldsymbol{E}_3, \boldsymbol{E}_4]^T$ and $\boldsymbol{v} = [\boldsymbol{z}, \boldsymbol{q}, \boldsymbol{s}, \boldsymbol{t}]^T$.

B. Solution Paradigm

In this paper, a novel solution paradigm has been employed in order to solve the MO problem formalized in (10). The idea, which originates from [13], [14], is based on the dynamic system theory. Briefly, it consists in developing an artificial stable dynamic system whose equilibrium point coincides with the solution of the considered MO problem. The Lyapunov theorem assures the stability of the afore–mentioned dynamic system. The reader is referred to [13]-[15] for further details.

IV. Case Studies

In this Section, the evaluation of the optimal number of subareas n^* is firstly performed for a cylindrical conductor characterized by a fixed set of parameters $\boldsymbol{p} = [L, h, r, \theta]^T$ (see Fig. 1).

A parametric analysis is then presented, with the aim of assessing the dependency of n^* on some constitutive parameter of the considered grounding electrode (simulation results suggest that the predicted n is quite insensitive to the electrode burial angle θ).

In order to show the validity of the proposed approach, predictions provided by the numerical simulation of the MaSM based model (employing the optimal number of subareas) have been compared, for each considered case, with results obtained through a software employing models based on the Finite Element Method (FEM) [16], [17].

Both FEM and MaSM based software tools used for the study reported in this work have been experimentally validated in [18].

A. Cylindrical Electrode

For a cylindrical electrode like the one depicted in Fig. 1, it is possible to recast the objective function vector (9) as follows:

$$\begin{cases} E_1 = f_1 - q_1 = \dfrac{L}{n} - q_1 \\ E_2 = f_2 - q_2 = \dfrac{n}{(n-1)L} - q_2 \\ E_3 = f_3 - q_3 = \dfrac{1}{\sqrt{k_1^2 L^2 + h^2 - 2hLk_1 \cos\left(\frac{\pi}{2} + \theta\right)}} - q_3 \\ E_4 = f_4 - q_4 = \dfrac{1}{\sqrt{k_2^2 L^2 + h^2 - 2hLk_2 \cos\left(\frac{\pi}{2} + \theta\right)}} - q_4 \\ E_5 = f_5 - q_5 = \sqrt{k_2^2 L^2 + r^2} - q_5 \\ E_6 = \dfrac{L}{nr} - s - 6 \qquad \text{with } s \ge 0 \end{cases} \quad (11)$$

where it has been considered:

$$\boldsymbol{f} = [f_1, f_2, f_3, f_4, f_5]^T = \left[\frac{1}{Acc_1}, \frac{1}{Acc_2}, \frac{1}{Acc_3}, \frac{1}{Acc_4}, \frac{1}{Acc_5}\right]^T , \quad (12)$$

and E_6 expresses, in form of equality constraint (Interior Point theory), the upper bound $L / n > 6r$ [7].

By setting:

$$\begin{cases} \boldsymbol{E} = [E_1, E_2, E_3, E_4, E_5, E_6]^T \\ \boldsymbol{q} = [q_1, q_2, q_3, q_4, q_5]^T \\ \boldsymbol{v} = [n, \boldsymbol{q}^T, s]^T \end{cases} , \quad (13)$$

through the solution paradigm presented in [13]-[15], it is possible to evaluate the zeros of (10).

Fig. 3 shows the trajectories $n(t)$, $f_1(t)$ and $q_1(t)$. It is important to remember that time t is a fictitious parameter. The only point of interest is the value assumed by the unknown quantities at the equilibrium ($t \to \infty$). As expected, $f_1(\infty) = q_1(\infty)$.

The obtained solution, which is reported in Table 1, verifies (7), therefore:

$$f_i^* = q_i^* \qquad \text{with} \qquad i = 1, 2, \dots, 5 \quad . \quad (14)$$

Since each q_i^* coincides with the minimum of f_i, the quantity:

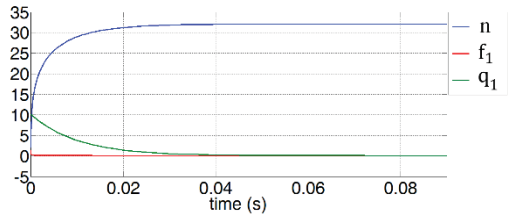

Fig. 3. Trajectories of n and q_1 from their initial values to the equilibrium.

$$\|\boldsymbol{q}^*\|^2 = (\boldsymbol{q}^*)^T \boldsymbol{q}^* \tag{15}$$

represents the minimum in L^2-norm of $\boldsymbol{f}$. As a consequence of the reasons that led to the formulation of $\boldsymbol{f}$, (15) can be assumed as the minimum of inaccuracy. Therefore, its reciprocal is a measure of the accuracy.

Considering that its absolute value is not meaningful for the purposes of this paper, for a more redable representation of the results, the accuracy has been defined as:

$$Acc = \frac{1}{\|\boldsymbol{q}^*\|^2} \cdot 1000 \tag{16}$$

Table 1 reports the value of the accuracy for the considered case study.

TABLE I. COMPUTATION FOR A CYLINDRICAL ELECTRODE

Electrode constitutive parameters			
$L = 3.048\ m$	$r = 0.007\ m$	$h = 0.1524\ m$	$\theta = 0.0\ rad$

Computed solution							
n^*	q_1^*	q_2^*	q_3^*	q_4^*	q_5^*	s^*	Acc
32.34	0.09	0.34	0.33	6.27	0.05	7.46	25.20

B. Parametric Analysis

In this section a parametric analysis, aimed at assessing the dependence of n^* on each electrode constitutive parameter (see Fig. 1), is reported.

Quantity μ, which is an index of the refinement degree associated with the particular subdivision adopted for the considered electrode, has been defined as follows:

$$\mu\left(\frac{n}{L}\right) = \frac{2r}{l} = \frac{2nr}{L} \tag{17}$$

The analysis is conducted varying, one at a time, each of the four parameters L, h, r and θ. Results are represented in the following Fig. 4-7.

The analysis of the reported curves allows for some interesting considerations:

- the number of subdivisions predicted by the MO process increases, with a nonlinear shape, as the length of the electrode increases. Fig. 4 shows that, for higher$L$, it is possible to use a lower number of subdivision per unit length keeping the accuracy roughly constant;

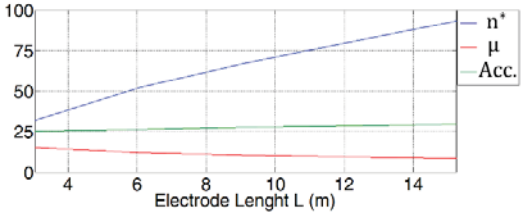

Fig. 4. Sensitivity of n^* with respect to electrode's lenght variations. Fixed parameters: $h = 0.1524$ m, $r = 0.007$ m and $\theta = 0.0$ rad.

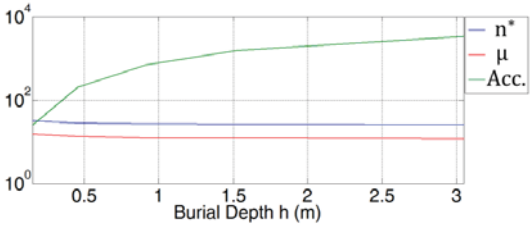

Fig. 5. Sensitivity of n^* with respect to electrode's burial depth variations. Fixed parameters: $L = 3.048$ m, $r = 0.007$ m and $\theta = 0.0$ rad.

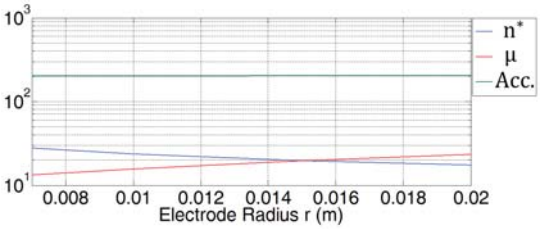

Fig. 6. Sensitivity of n^* with respect to electrode's radius variations. Fixed parameters: $L = 3.048$ m, $h = 0.4572$ m and $\theta = 0.0$ rad.

- as the burial depth h increases (Fig. 5), the predicted n^* slightly decreases, whereas the accuracy increases. This is in agreement with the fact that the propagation of the potential error from the boundary of the conductor goes from a maximum (at the boundary) to zero at infinity [8]. So, for a fixed n, the accuracy on the evaluation of potential on the soil surface must increase accordingly with h (Fig. 5).

C. Validation of the Results

For each case presented in Fig. 4-7, values of the earth resistance R_E and the electric potential on some points of the soil surface (see Fig. 1) are computed by an algorithm, written in MATLAB®, based on the MaSM [18], [19]. The number of subareas adopted for each configuration is the one predicted by the MO process.

Obtained results are then compared with those computed with a software based on the FEM.

The FEM has been used to study the effects of the considered electrodes on a finite volume of soil, delimited by a hemispheric boundary of radius:

$$r_e = 6L \tag{18}$$

The number of tetrahedral mesh elements adopted in order to discretize the considered domain varies from case to case: from a minimum of 0.7e6 to a maximum of 1.6e6 (which can be considered high enough to guarantee an extra fine mesh and therefore a good solution). No symmetry conditions are imposed.

The space outside the hemisphere is modelled as a resistance equal to the earth resistance of a hemispherical electrode of radius r_e [5].

In all simulated cases, soil is modelled as a homogeneous medium (resistivity $\rho = 100$ Ωm) and the leakage current is $I_F = 1$ A.

Fig. 9-12 report the results obtained with both methods.

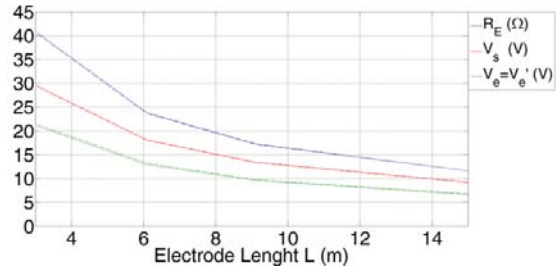

Fig. 9. Comparison between quantities computed adopting n^* with MaSM (solid lines) and those computed with FEM (dashed lines). Electrode's fixed parameters: $h = 0.1524$ m, $r = 0.007$ m and $\theta = 0.0$ rad.

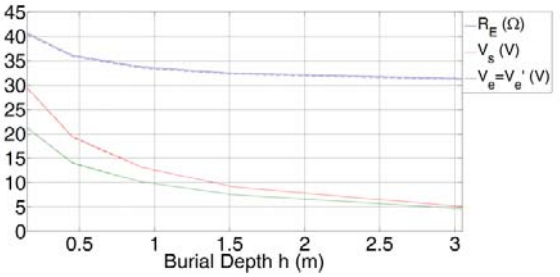

Fig. 10. Comparison between quantities computed adopting n^* with MaSM (solid lines) and those computed with FEM (dashed lines). Electrode's fixed parameters: $L = 3.048$ m, $r = 0.007$ m and $\theta = 0.0$ rad.

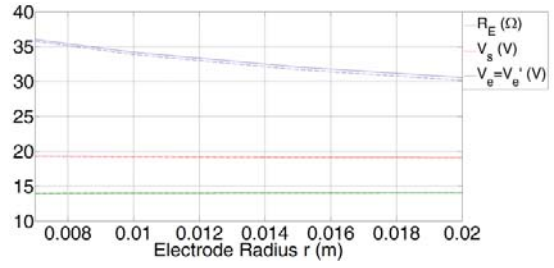

Fig. 11. Comparison between quantities computed adopting n^* with MaSM (solid lines) and those computed with FEM (dashed lines). Electrode's fixed parameters: $L = 3.048$ m, $h = 0.4572$ m and $\theta = 0.0$ rad.

The comparison shows a very good agreement, in fact the distances between curves are inappreciable in the ordinary scale. Relative errors never exceed 2.2%.

In order to evaluate how the number of subareas affects the model predictions, Fig. 13 and 14 report values of R_E and potential V_e' (see Fig. 1) for a cylindrical electrode characterized by parameters reported in Table 3. Quantities were computed with MaSM, performing iterative simulations with n varying from 1 to 550 (thin blue lines). Figures also report, as a reference, the FEM computed values (thick blue lines).

With reference to the simulation for $n = n^*$, the reduction in MaSM computational time (ΔCPU_{time}), for each n, is shown in Fig. 13 (green line).

Fig. 14 also reports the percentage relative error of V_e' computed with MaSM (green line), with reference to the value provided by FEM simulation.

TABLE II. COMPUTATION FOR A CYLINDRICAL ELECTRODE (REF. FIG. 1)

Electrode constitutive parameters			
$L = 50m$	$r = 0.05m$	$h = 0.5m$	$\theta = 0.0\ rad$
Soil resistivity		Leackage current	
$\rho = 100\ \Omega m$		$I_F = 1\ A$	

Computed solution				
n^*	**MaSM**		**FEM**	
71	R_E^* [Ω]	$V_e'^*$ [V]	R_E [Ω]	V_e' [V]
	33.2247	2.0349	33.2134	2.0423

It can be seen that both R_E and V_e', computed with MaSM, depends on n, although to different degrees.

Variations of R_E are, in fact, in a short range (≤7%), whereas changes in V_e' can be more consistent (≤18%).

So, even if it is not very relevant for the determination of R_E (as already highlighted in previous studies [8]), the choice of a particularly small value of n can determine consistent errors when it comes to evaluate potentials on the soil surface.

It is important to underline that knowing a priori, case by case, if a chosen n is suitable for the grounding electrode under examination is not possible.

At this purpose, iterative simulations (at least two), varying the number of subareas, must be accomplished [6], [7], [9], [19]. This may become a very onerous task for complex grounding systems, which are made up by a great number of interconnected leaking elements (and therefore, a great number of overall subareas). Computational time, in fact, considerably increases with the number of subareas, as can be seen in Fig. 13.

Values R_E^* and $V_e'^*$ in Fig. 13 and 14 (red marks) represent the quantities evaluated adopting the n^* predicted by MO process. It is evident how close they are to the condition of minimum distance from FEM computed reference values.

The presented procedure allows, therefore, the knowledge, in "one shot", of the number of subareas that guarantees reliable results.

V. CONCLUSION

The number n of subareas in which a grounding electrode is divided when applying the MaSM has an impact on

computation time and on the accuracy of the model predictions (in particular those related to the ground surface potentials). Usually n is chosen empirically or using iterative methods, which imply multiple runs of the MaSM calculation tool. This paper presents a method for evaluating the optimal number of subareas n^* that has to be chosen in order to properly model a grounding electrode, with reference to its position and its constitutive parameters.

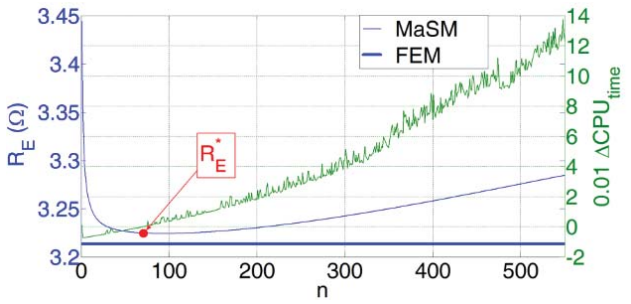

Fig. 13. Proximity of R_E^*, evaluated adopting n^* , to the condition of minimum distance from FEM computed value. Computational time percentage reduction, with reference to the simulation carried out for $n = n^*$ (green line).

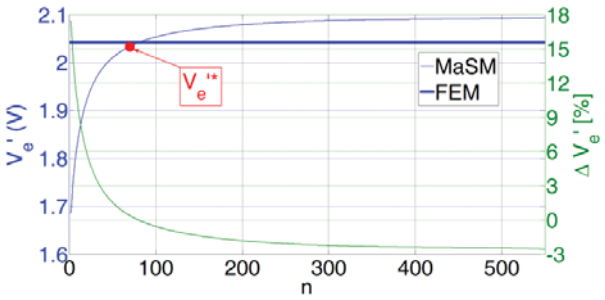

Fig. 14. Proximity of $V_e'^*$, evaluated adopting n^*, to the condition of minimum distance from FEM computed value. Percent relative error of V_e' computed with MaSM, with reference to FEM reference one (green line).

Thanks to this method, n^* can be obtained with a single and fast calculation, based on the characteristics of the electrode, thus avoiding the burden of iterative runs of the MaSM calculation tool (particularly critical in case of complex grounding systems).

The method has been applied to a simple test case and the results show that the calculated n^* provides a very good tradeoff between computation time and accuracy of the results. In fact, the number of subareas n^* ensures, case by case, results close to the condition of minimum distance from FEM computed ones (assumed as reference). It is also showed that increasing n beyond n^* does not provide any advantage.

ACKNOWLEDGMENT

This work was supported by Cassa Conguaglio per il Settore Elettrico - now Cassa per i Servizi Energetici e Ambientali (CSEA) - in the framework of the Meterglob project.

REFERENCES

[1] J.C.Maxwell, A Treatise On Electricity and Magnetism, vol. 2. New York: Dover Publications, 1954.

[2] E.D.Sunde, Earth Conduction Effects in trasmission systems. New York: Dover publications, 1968

[3] P.Buccheri, V.Cataliotti, G.Morana, “Calcolo automatico di impianti di terra comunque complessi in terreni omogenei e non omogenei a doppio strato”, L’Energia Elettrica, no. 6, 1977.

[4] V. Cataliotti, A. Campoccia, Impianti di Terra, Torino: TNE, 2011, pp. 75-77.

[5] F.Freschi, M.Mitolo, M.Tartaglia, “An Effective Semianalytical Method for simulating Grounding Grids”, IEEE Trans Idustry Applications, vol. 49, no. 1, Jan/Feb 2013.

[6] D.L.Garret, J.G.Pruitt, “Problems encountered with the average potential method of analyzing substation grounding systems”, IEEE Trans. Power App. Syst., vol. PAS-104, pp.3586-3596, Dec. 1985.

[7] E.B.Joy, R.E.Wilson, “Accuracy study of the ground grid analysis algorithm”, IEEE Trans. Power Delivery, vol. PWRD-1, pp. 97-103, July 1986.

[8] Y.L.Chow, M.M.Elsherbiny, M.M.A. Salama, “Earth surface Voltages at a Grounding System of Buried Grid and Rods from the Fast Galerkin’s Moment Method”, presented at Canadian Conf. on Electrical and Computer Engineering, Sept 1995.

[9] M.Sylos Labini, A.Covitti, S.De Nisi, F.Laddomada, “A Fuzzy-Maxwell combined method for simplifying the -calculation of the current field generated by a cylindrical electrode”, IEEE Trans. On Magnetics, vol. 36, no. 4, pp. 708-711, July 2000.

[10] H. Wei, H.Sasaki, J.Kubokawa and R. Yokoyama, “An interior point nonlinear programming for optimal power flow problems with a novel data structure”, IEEE Trans. Power Apparat. Syst., vol. 13, pp. 870-877, Aug. 1998.

[11] G.L.Torres, V.H.Quintana, “An interior-point method for nonlinear optimal power flow using voltage rectangular coordinates”, IEEE Trans. Power Apparat. Syst., vol. 13, pp. 1211-1218, Nov. 1998.

[12] J.A.Momoh, J.Z. Zhu, “Improved interior point method for OPF problems”, IEEE Trans. Power Apparat. Syst., vol. 14, pp.1114-1120, Aug. 1990.

[13] Xie N., Torelli F., Bompard E., Vaccaro A. (2013). A generalized computing paradigm based on artificial dynamic models for mathematical programming. IET Generation, Transmission and Distribution, Vol.7(8).

[14] Torelli F. and Vaccaro A. (2014). A generalized computing paradigm based on artificial dynamic models for mathematical programming. Soft Computing, Vol. 18(8), pp. 1561–1573

[15] F. Torelli, A. Vaccaro and N. Xie, “A Novel Optimal Power Flow Formulation Based on the Lyapunov Theory”, IEEE Trans. Power Systems, Vol. 28, n. 4, pp. 4405-4415, Nov. 2013.

[16] J. Nahman and I. Paunovic, “Mesh voltages at earthing grids buried in multi-layer soil,” Electric Power Systems Research, vol. 80, no. 5, pp. 556-561, 2010.

[17] V. L. Coelho, A. Piantini, H. A. Almaguer, R. A. Coelho, W. do C. Boaventura, and J. O. S. Paulino, “The influence of seasonal soil moisture on the behavior of soil resistivity and power distribution grounding systems,” Electric Power Systems Research, vol. 118, pp. 76-82, 2015.

[18] Pons, E.; Colella, P.; Tommasini, R.; Napoli, R.; Montegiglio, P.; Cafaro, G.; Torelli, F., "Global Earthing System: Can Buried Metallic Structures Significantly Modify the Ground Potential Profile?," Industry Applications, IEEE Transactions on , vol. 51, Issue 6, pp. 5237-5246, 2015.

[19] G. Cafaro, P. Montegiglio, F. Torelli, A. Barresi, P. Colella, A. De Simone, M. Di Silvestre, L. Martirano, E. Morozova, R. Napoli, G. Parise, L. Parise, E. Pons, E. Riva Sanseverino, R. Tommasini, F. Tummolillo, G. Valtorta and G. Zizzo, “Influence of LV neutral grounding on global earthing systems,” Industry Applications, IEEE Transactions on, Vol. 53, Issue 1, pp. 22-31, 2016.